sciendo Applied Mathematics and Nonlinear Sciences, 9(1) (2024) 1-14

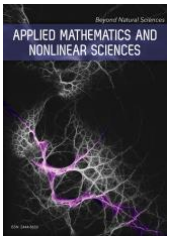

Applied Mathematics and Nonlinear Sciences

https://www.sciendo.com

Impact toughness analysis of offshore wind power structures under the influence of long-period waves

Senhui Jiang[1,†], Qing Wang[1]

1. College of Civil Engineering and Engineering Management, Guangzhou Maritime University, Guangzhou, Guangdong, 510725, China.

Submission Info

Communicated by Z. Sabir
Received January 12, 2024
Accepted January 19, 2024
Available online February 26, 2024

Abstract

In this paper, the performance of offshore wind turbine structures under long-period wave impacts is investigated, and a numerical model of long-period waves is developed to simulate the wave motion and fluid seepage in the pore medium by using the VARANS equation with the OlaFlow solver, and various turbulence models such as the model, RNG model, and the VOF method is applied to capture free surfaces, which can accurately simulate wave generation, propagation, reflection, breaking, and fluid seepage in the pore medium. These methods can accurately simulate the wave generation, propagation, reflection, breaking, and fluid seepage in the pore medium, and the accuracy of the numerical simulation is verified by comparing the results with those of the physical experiment. The results show that the wind farm exhibits good impact toughness under the influence of long period waves, and its overturning stability and slip stability are better than the safety coefficient required by the specification.

Keywords: OlaFlow; VARANSOF; Wave modeling; Impact toughness.
AMS 2010 codes: 68T01

†Corresponding author.
Email address: jiangsh_gmi@163.com

ISSN 2444-8656
https://doi.org/10.2478/amns-2024-0534

1 Introduction

As a kind of clean energy, the proportion of offshore wind power in the global energy structure continues to rise [1]. However, offshore wind power platforms are exposed to complex marine environments all year round, especially the long period wave, which poses a serious challenge to their structural stability [2]. Therefore, an in-depth understanding of the impact and toughness effects of the period wave on the offshore wind power structure is crucial to guarantee the safe operation of offshore wind power [3-4]. The impact toughness of long-period waves on offshore wind power structures is crucial to ensure the safe operation of offshore wind power.

Long-period waves usually refer to waves with a wave period of more than 12 seconds, which have the characteristics of high energy and wavelength [5]. They have small energy loss when traveling in the deep ocean, and once approaching the coastline or wind power platform area, the energy is rapidly concentrated, causing a huge impact on the offshore structure [6]. The impact of long-period waves on the offshore wind power structure is mainly reflected in the mechanical impact and fatigue damage on the tower, foundation, and blades [7]. The impact of long-period waves on the offshore wind power structure is mainly reflected in the mechanical impact and fatigue damage on the tower, foundation, and blades [8]. The impact on the offshore wind power structure is mainly reflected in the mechanical impact and fatigue damage on the tower, foundation, and blades [9]. The impact toughness of offshore wind power structures refers to their ability to resist damage and maintain functionality in extreme environments such as long-period waves, which not only depends on the physical properties of the structural materials but also involves the design, installation, and operation and maintenance of many aspects [10]. Improving the impact toughness of the structure can effectively prolong the service life of the wind power platform and reduce the maintenance cost [11].

The related research mainly adopts the combination of computational fluid dynamics (CFD) simulation and actual marine environment testing [12]. Through simulation analysis, the distribution of the impact force and the possible damage area of the wind power structure by the long-period wave can be predicted [13]. At the same time, combined with the test data of the actual marine environment, the simulation results can be verified, and the actual impact toughness assessment can be carried out [14]. By optimizing the tower and foundation structure, the impact toughness of the tower and foundation structure can be improved, which can effectively prolong the service life of the wind power platform and reduce the maintenance cost. By optimizing the structural design of the tower and foundation, such as using more ductile materials and increasing the redundancy of the structure, the resistance of the structure to the impact of long-period waves can be improved [15]. By selecting areas with relatively small wave impacts for the installation of wind power platforms or using topography to reduce the effect of wave energy, the impact of long-period waves can be reduced [16-17]. At the same time, a real-time monitoring system is established to predict and monitor the long-period wave activities so that early warning and countermeasures can be taken [18-19], and then adaptive maintenance strategies are formulated and implemented according to the actual impacts of long-period waves on the structure in order to maintain the stability and safety of the structure [20].

The study of the impact toughness of long-period waves on offshore wind power structures is of great significance in ensuring the safe operation and economic benefits of wind power platforms [21]. The toughness and durability of offshore wind power structures can be significantly improved by optimizing the design, siting, monitoring, and maintenance strategies.

In this paper, a numerical model of long-period waves is developed, and OlaFlow is used as the solver to form the VARANS equation with the continuity equation and the momentum conservation equation, and the commonly used turbulence models, including the model and the RNG model, are investigated, and the VOF method is used to capture the free surface, and a volume function is introduced to

determine the free surface, i.e., the fraction of the volume of the water in each cell, to simulate the wave-seabed-structure interaction process, and the Stokes I and II order wave-making methods are used to realize the accurate wave-making process. To simulate the wave-seabed-structure interaction process, the Stokes I and II wave-making methods are adopted to realize accurate wave-making, and the active wave cancellation method is adopted to offset the waves by applying the corresponding velocity at the outlet boundary. In the evaluation of wave impact toughness in offshore wind farms, the wave model is used to check the stability of capsize and slip resistance.

2 Numerical modeling of wave impact problems

Under the basic assumption of incompressibility of fluid, various numerical models of nonlinear wave deformation and its effect on structures can be categorized into two main types: the potential flow model and the viscous flow model.

2.1 Potential Flow Model (PFM)

The potential flow model (neglecting viscosity) is mainly used for the calculation of wave loads on large-scale ($ka \geq O(1)$ (a is the characteristic scale of the structure and k is the wave number) oceanographic structures. In the potential flow model, the problem is still accurately expressed in terms of the laws of conservation of mass (which are transformed into the form of Laplace's equations) and momentum (which are transformed into the form of Bernoulli's equations and are used as dynamic boundary conditions at the free surface) and boundary conditions. (into the form of Bernoulli's Equation and as a dynamic boundary condition at the free surface) and boundary conditions.

Consider a rectangular wave pool model; the upstream boundary in the x direction is given as an incident regular wave condition, the downstream boundary is set as an open boundary condition, there is a fixed structure piercing the water surface in the pool, and the fluid is set to be ideal and incompressible, and the margin problem on the three-dimensional Laplace equation expressed in terms of a velocity potential function, $\Phi(x, y, z, t)$, is to satisfy within the fluid region, Ω, the following:

$$\nabla^2 \Phi(x, y, z, t) = 0 \tag{1}$$

The kinetic and kinematic conditions are satisfied on the free surface boundary Γ_f:

$$\frac{\partial \Phi}{\partial t} + \frac{1}{2} \nabla \Phi \cdot \nabla \Phi + g\eta = 0 \tag{2}$$

$$\frac{\partial \Phi}{\partial z} = \frac{d\eta}{dt} \tag{3}$$

Boundary conditions on the poolside interfaces, a bottom surface, upstream wave-making boundary surfaces, and fixed structural wall surfaces in the pool (these boundary surfaces are uniformly represented by Γ_s) are:

$$\frac{\partial \Phi}{\partial n} = V_n(t) \tag{4}$$

V_n Is the pre-given normal velocity at any point on the boundary plane for the upstream wave-making boundary; if the cosine wave is given as the condition of the incident wave, then the normal velocity $V_n(t)$ varies according to the given sinusoidal form and $V_n(t)=0$ is generally taken on the other boundary planes represented by the Γ_s.

Sommerfeld-Orlanski (S-O) radiation conditions are generally given on the open boundary surface Γ_r downstream of the pool:

$$\frac{\partial \Phi}{\partial t}+C\frac{\partial \Phi}{\partial n}=0 \tag{5}$$

In addition, wave attenuation is also carried out in the numerical wave flume (pool) opening boundary treatment by setting up a sponge layer before opening the boundary so as to minimize the wave energy reaching the boundary.

The numerical realization of the potential flow model mainly relies on the boundary element method to numerically solve the boundary integral equation:

$$\frac{1}{4\pi}\int_{\Gamma}\left[G(p,q)\frac{\partial \Phi(q)}{\partial n(q)}-\Phi(q)\frac{\partial G(p,q)}{\partial n(q)}\right]d\Gamma_q=C(p)\Phi(p),\ p\in\Gamma \tag{6}$$

Here, $\Gamma=\Gamma_f\cup\Gamma_s\cup\Gamma_r, p=(x,y,z)\in\Gamma, q=(\xi_1,\xi_2,\xi_3)\in\Gamma, G(p,q)$ is the Green's function, and $C(p)$ is a coefficient related to the unit profile and the shape of the region.

There are many research works on wave-structure interactions applying potential flow models and BEMs, e.g., the hybrid Eulerian-Lagrangian H-process for solving the boundary integral equation (BIE) was proposed by Longuet-Higgins & Cokelet, the two-dimensional wave-body interaction problem was investigated by Clement, and on the 3D side, there is the nonlinear axisymmetric flow with a free Nonlinear axisymmetric flow with free surfaces, Beck et al. Compared with in-domain discretization methods (e.g., finite difference), BEM only requires discretization of the boundary of the computational domain and thus has the advantage of having a small number of discretization points and directly giving the location of the transient free surfaces; however, the computational cost of BEM is still quite high, because BEM has to pay high computational costs (in terms of the cost of the coefficient matrix of unknowns in the linear system of equations and a full matrix at the end of the system). The size of the computational domain of the BEM model for solving three-dimensional nonlinear hydrodynamic problems is still severely limited by the fact that the BEM model can be used to solve the problem in the time domain, and the size of the computational domain of the BEM model for solving three-dimensional nonlinear hydrodynamic problems is still limited by the fact that the BEM model can be used to solve the problem in the time domain. Constraints.

2.2 Viscous Flow Model

In the viscous flow model of waves, the fundamental conservation laws that govern real fluid flow - conservation of mass and conservation of momentum - are described by the following continuity and Navier-Stokes (N-S) equations, respectively.

Continuity equation.

$$\nabla \cdot \mathbf{u} = 0 \tag{7}$$

N-S equation.

$$\left(\frac{\partial}{\partial t} + \mathbf{u} \cdot \nabla\right)\mathbf{u} = -\nabla\left(\frac{P}{\rho} + gz\right) + v\nabla^2\mathbf{u} \tag{8}$$

3 Long-period wave model

The solver used for the wave model is OlaFlow, which was developed by Higuera et al. based on the standard solver InterFoam in OpenFOAM. OlaFlow is used to control the wave motion and the seepage of the fluid in the pore medium by solving the VARANS equations, and the turbulence models are such as the VARANS model and the RNG model, etc., and the VOF method is used to capture the free surface.

3.1 Control Equation

The controlling Equation is the VARANS equation, which consists of a continuity equation and a momentum conservation equation and is applicable to most practical offshore engineering problems using the assumption of an incompressible fluid.

$$\frac{\partial \langle u_i \rangle}{\partial x_i} = 0 \tag{9}$$

$$\frac{\partial \rho \langle u_i \rangle}{\partial t} + \frac{\partial}{\partial x_j}\left[\frac{1}{\varnothing}\rho \langle u_i \rangle \langle u_j \rangle\right] = -\varnothing \frac{\partial \langle p^* \rangle f}{\partial x_i} + \varnothing g_j X_j \frac{\partial \rho}{\partial x_i} + \frac{\partial}{\partial x_j}\left[\mu_{eff} \frac{\partial \langle u_i \rangle}{\partial x_j}\right] - [CT] \tag{10}$$

$$[CT] = A\langle u_i \rangle + B|\langle u \rangle|\langle u_i \rangle + C\frac{\partial \langle u_i \rangle}{\partial t} \tag{11}$$

The coefficients A and B in Equation (11) are calculated according to the formula proposed by Engelund and improved by Van Gent as follows.

$$A = \alpha \frac{(1-\varnothing)^3}{\varnothing^2}\frac{\mu}{D_{50}^2} \tag{12}$$

$$B = \beta\left(1 + \frac{7.5}{KC}\right)\frac{1-\varnothing}{\varnothing^2}\frac{\rho}{D_{50}} \tag{13}$$

Where $\langle\rangle$ denotes volume average, ρ denotes density, u_i denotes velocity vector, $p*$ denotes proposed kinetic pressure, g_i denotes gravitational acceleration, X is the position vector, $\varnothing$ denotes the porosity of the pore material, D_{50} denotes the average equivalent particle size of the pore material, α is the index (VOF) function, and μ_{eff} denotes the effective kinetic viscosity, which takes into account the molecular kinematic viscosity plus turbulence effect $\mu_{eff} = \mu + \rho v_t$, v_t is the turbulence kinematic viscosity and is given by the selected turbulence model.

3.2 Turbulence models

Commonly used turbulence models include the $k-\varepsilon$ model and the RNG $k-\varepsilon$ model, etc. Among them, the turbulence model is more widely used in computational fluid dynamics. The detailed expression of the $k-\varepsilon$ turbulence model is as follows:

$$k=\frac{\overline{U'U'}}{2} \tag{14}$$

$$\varepsilon=\frac{C_{\mu}^{0.75}k^{1.5}}{l} \tag{15}$$

$$\frac{\partial k}{\partial t}+\nabla\cdot(kU)-\nabla\cdot\left[\left(v+v_t\right)\right]\nabla k=v_t\left[\frac{1}{2}\left(\nabla U+\nabla U^T\right)\right]^2-\varepsilon \tag{16}$$

$$\frac{\partial \varepsilon}{\partial t}+\nabla\cdot(\varepsilon U)-\varepsilon\nabla\cdot U-\nabla\cdot\left[\left(v+\frac{v_t}{\sigma_{\varepsilon}}\right)\right]\nabla k=2C_1v_t\left[\frac{1}{2}\left(\nabla U+\nabla U^T\right)\right]^2\frac{\varepsilon}{k}-\frac{C_2\varepsilon^2}{k} \tag{17}$$

Where k stands for turbulent kinetic energy, ε stands for turbulent dissipation rate, U' stands for pulsation velocity, $\overline{U'}$ stands for pulsation velocity after averaging at Reynolds time, and the turbulent kinematic viscosity v_t is calculated as:

$$v_t=C_{\mu}\frac{k^2}{\varepsilon} \tag{18}$$

The coefficients C_1, C_2, C_{μ} and σ_{ε} in the $k-\varepsilon$ turbulence model are generally based on empirical data.

$k-\varepsilon$ turbulence model assumes that the turbulent viscosity is isotropic, which is good at dealing with the case of small pressure gradient, but for the case of large pressure gradient, the $k-\varepsilon$ model is less effective, therefore, some scholars based on the idea of reorganization of the group, the $k-\varepsilon$ model is modified, the RNG $k-\varepsilon$ model, which overcomes the problems of the standard RNG $k-\varepsilon$ model, the RNG $k-\varepsilon$ turbulence model is based on the following equations:

$$\frac{\partial(\rho k)}{\partial t}+\frac{\partial\left(\rho k u_i\right)}{\partial x_i}=\frac{\partial}{\partial x_j}\left(\alpha_k\mu_{eff}\frac{\partial k}{\partial x_j}\right)+G_k-\rho\varepsilon \tag{19}$$

$$\frac{\partial(\rho\varepsilon)}{\partial t}+\frac{\partial\left(\rho\varepsilon u_i\right)}{\partial x_i}=\frac{\partial}{\partial x_j}\left(\alpha_{\varepsilon}\mu_{eff}\frac{\partial \varepsilon}{\partial x_j}\right)+\frac{C_{1\varepsilon}^*}{k}G_k-C_{2\varepsilon}\rho\frac{\varepsilon^2}{k} \tag{20}$$

The $k-\varepsilon$ turbulence model was used in the model validation section.

3.3 VOF method for tracing free surfaces

The wave model uses the VOF method to capture the free surface. The VOF method determines the free surface by introducing the volume function α, which is defined as the volume fraction of water

in each cell. This means that, $\alpha = 1$ represents a grid cell filled with water, $\alpha = 0$ represents a cell filled with air, and $0 < \alpha < 1$, is denoted as the free surface of the fluid. That is:

$$\alpha = \begin{cases} 0 & \text{Air} \\ 0 < \alpha < 1 & \text{Free surface} \\ 1 & \text{Water} \end{cases} \tag{21}$$

In this way, it is simple to calculate any property of the fluid in each grid cell by simply weighting them with the VOF function. e.g., the cell density and the effective kinetic viscosity in a fluid grid are calculated as follows:

$$\rho = \alpha \rho_{water} + (1-\alpha)\rho_{air} \tag{22}$$

$$\mu_{eff} = \alpha \mu_{eff\ water} + (1-\alpha)\mu_{eff\ air} \tag{23}$$

The volume function needs to satisfy the convection equation:

$$\frac{\partial \alpha}{\partial t} + \frac{1}{\varnothing}\frac{\partial \langle u_i \rangle \alpha}{\partial x_i} = 0 \tag{24}$$

$$\frac{\partial \alpha}{\partial t} + \frac{1}{\varnothing}\frac{\partial \langle u_i \rangle \alpha}{\partial x_i} + \frac{1}{\varnothing}\frac{\partial \langle u_{ci} \rangle \alpha(1-\alpha)}{\partial x_i} = 0 \tag{25}$$

3.4 Numerical wave generation

Accurate wave generation is the basis for modeling wave-seabed-structure interaction, and if the generated waves are inaccurate, the whole calculation process may deviate completely from the actual situation. Wave generation methods include Stokes I, II, V, elliptic cosine wave isolated wave, etc. Here, we mainly adopt the Stokes I and II order wave generation methods.

The wavelength of the Stokes I wave is given by:

$$L = \frac{gT^2}{2\pi}\tanh\left(\frac{2\pi h}{L}\right) = 0 \tag{26}$$

$$k = \frac{2\pi}{L} \tag{27}$$

$$\omega = \frac{2\pi}{T} \tag{28}$$

$$c = \frac{L}{T} \tag{29}$$

$$L_0 = \frac{gT^2}{2\pi} \tag{30}$$

Where T is the period, k is the wave number, h is the water depth, ω is the frequency, c is the wave speed, and L_0 is the wavelength of deep water waves?

The solution of the theory is based on a potential function from which the elevation of the free surface and the velocity field can be obtained. For a two-dimensional wave propagating along the x-axis, the elevation of the free surface and the velocities in the x- and z-directions can be expressed as follows:

$$\eta = \frac{H}{2}\cos(kx - \omega t + \psi) = 0 \tag{31}$$

$$u = \frac{H}{2}\omega\frac{\cosh(kz)}{\sinh(kh)}\cos(kx - \omega t + \psi) = 0 \tag{32}$$

$$w = \frac{H}{2}\omega\frac{\sinh(kz)}{\sinh(kh)}\cos(kx - \omega t + \psi) = 0 \tag{33}$$

Where η represents the free surface elevation, H is the wave height, u represents the horizontal velocity, w represents the vertical velocity, and φ is the phase angle.

Stokes's second-order wave theory is based on the introduction of second-order terms in the I. The equations for the free surface elevation η, horizontal velocity u and vertical velocity w are as follows:

$$\eta = \frac{H}{2}\cos(\theta) + k\frac{H^2}{4}\frac{3-\sigma^2}{4\sigma^3}\cos(2\theta) \tag{34}$$

$$u = \frac{H}{2}\omega\frac{\cosh(kz)}{\sinh(kh)}\cos(\theta) + \frac{3}{4}\frac{H^2\omega k\cosh(2kz)}{4\sinh^4(kh)}\cos(2\theta) = 0 \tag{35}$$

$$w = \frac{H}{2}\omega\frac{\sinh(kz)}{\sinh(kh)}\cos(\theta) + \frac{3}{4}\frac{H^2\omega k\sinh(2kz)}{4\sinh^4(kh)}\sin(2\theta) = 0 \tag{36}$$

In which, $\sigma = \tan(kh)$.

3.5 Numerical Wave Dissipation

In the wave field simulation process, the wave will be reflected at the boundary. The reflected wave and the superposition of the incident wave will change the nature of the wave, so it is necessary to apply the wave elimination method to eliminate the reflected wave; the main elimination methods are radiation boundary elimination, artificial sponge layer elimination method, etc. The radiation boundary condition is through the absorption of wave energy at the boundary to achieve the purpose of elimination of the wave. In Equation (36), radiation boundary elimination needs to be known to the wave speed, so it is not suitable for multi-frequency waves.:

$$\frac{\partial\varphi}{\partial n} = -\frac{1}{c}\frac{\partial\varphi}{\partial t} \tag{37}$$

In order to overcome the shortcomings of the radial boundary condition dissipation method, the artificial sponge layer dissipation method is proposed, which is based on the addition of a damping dissipation term, $-f(x)\langle u_i \rangle$, to the momentum equation, and the dissipation is realized by increasing the damping dissipation term, and the u_i is the velocity component:

$$f(x) = \beta \frac{(x - x_1)}{|x_1 - x_2|} \tag{38}$$

Where β is the damping coefficient, x_1 and x_2 represent the locations of the starting point and the endpoint of the wave dissipation zone, respectively.

The wave model in this paper adopts the active wave dissipation method in wave dissipation by applying the corresponding speed on the exit boundary to realize the mutual offset of waves, and the wave dissipation effect is better.

4 Validation of numerical simulation against experimental results

In this section, the proposed wave model is applied to establish a numerical wave flume model, and the numerical simulation of the impact of long-period waves on offshore wind power structures is carried out, and the numerical results are compared with the actual simulation experiments to verify the numerical simulation and experimental results are shown in Fig. 1, which shows that, in the set long-period waves of 15-20, no matter the numerical simulation or the physical experiments, the wave impact force goes through the following process: firstly, it gradually rises, reaches the maximum impact extreme value, then gradually falls to 0 value, a relatively stable zero-value moment, and then it is followed by a relatively stable zero-value moment. It can be seen that, under the set long period wave of 15~20, no matter the numerical simulation or physical experiment, the impact force of the wave has gone through the following process: firstly, it rises gradually, reaches the extreme value of the maximum impact, and then gradually falls to 0, a relatively stable zero-value moment, and then enters into the next impact. The numerical simulation results of each group can reproduce this process well, and the numerical results for the simulation of the alternating process of the impact pressure are also consistent with the experimental values; the numerical simulation results are very close to the experimental values. The numerical simulation results are very close to the experimental values, and the oscillations of the impact pressure in the process of rising and falling due to the influence of the air phase are also reproduced in the numerical results. On the whole, the wave model proposed in this paper can simulate the long-period wave impacts encountered by the offshore wind turbine structure, and the simulation of the extreme values of the impact pressures on the offshore wind turbine structure and the time course of the pressures are in line with the experimental results of the physical model.

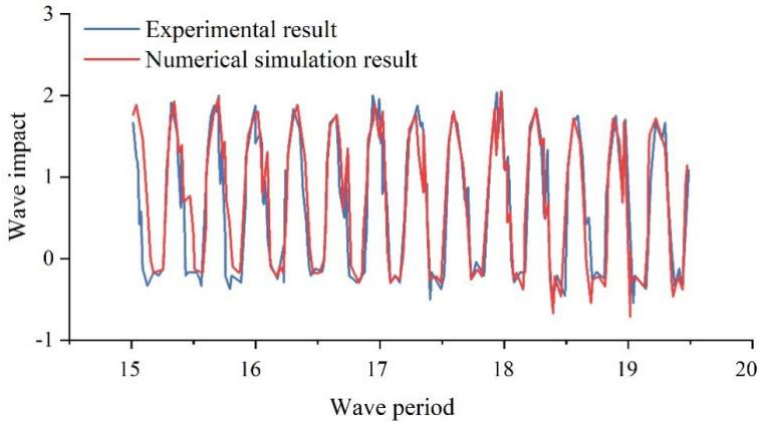

Figure 1. Numerical simulation and experimental results

5 Evaluation of wave impact toughness in offshore wind farms

In this chapter, the impact toughness of an offshore structure, a 202MW offshore wind farm off the coast of Langshui, Jiangsu Province, China, is investigated in the context of the wave model proposed in the paper when it is subjected to long-period wave impacts. The impact toughness consists of two aspects: overturning stability and slippage stability, which have a direct influence on the operational performance and safety of the platform and will be analyzed in the following.

5.1 Anticapsizing Stability

The tilting stability of offshore structures is measured according to the tilting moment and overturning moment of the platform, and the minimum value of the tilting safety coefficient of offshore wind farms is 1.4. When waves and currents are combined, assuming isotropic action, the five directions of action are taken as 0°, 64.2°, 90°, 180° and 244.2° respectively, and the tilting moments of offshore wind farms are shown in Table 1. As shown in Table 1, it can be seen that when the wave period is 12.52s and 13.31s, the overturning moments are maximum at 64.2° in the wave direction, which is 11112.2 and 8572.911, respectively, and when the wave period is 14.72s, the overturning moments are maximum at 180° in the wave direction, which is 7984.68, while the wave period is 15.68s, the overturning moments are maximum at 90° in the wave direction, which is 7984.68, respectively. The tilting moment at 90° of the wave direction is 6890.745, which is the largest among the five wave directions.

Table 1. Upsetting moment

Wave cycle(s)	Upsetting moment				
	0°	90°	64.2°	180°	244.2°
12.52	10101.98	10936.2	11112.2	10625.2	10625.2
13.31	8227.634	8406.08	8572.911	8101.815	8184.816
14.72	7628.785	7327.865	7543.255	7984.68	7851.748
15.68	6368.843	6890.745	6513.547	6401.303	6218.393

The tilting moments of offshore wind farms are shown in Table 2, and it is obvious that the minimum tilting moments of different wave periods correspond to the maximum overturning moments of different wave periods mentioned above, and the minimum tilting moments of wave direction 64.2° are 44922.3 and 30406.64 when the wave periods are 12.52s and 13.31s, respectively. At this time,

for the most dangerous situation of offshore wind farm tilt stability, the tilt stability calibration, respectively, can get the tilt safety factor, 4.03, 3.55, which are greater than 1.4 and higher than the norms of the tilt safety factor. When the wave period is 14.72s, the tilting moment in the direction of the wave 180 ° is the smallest, 21096.03, with a tilting safety factor of 2.74. In the wave period of 15.68s, the tilting moment is the smallest in the wave direction 180 °, 21096.03, and the tilt safety factor is 2.74. in the wave period of 15.68s, the tilting moment in the wave direction 15.68s, the wave period is the smallest. In the wave period of 15.68s, the tilting moment is minimized at 90° of wave direction, which is 20871.79, and the tilting safety coefficient is 3.03.

Table 2. Tipping moment

Wave cycle(s)	Tipping moment				
	0°	90°	64.2°	180°	244.2°
12.52	53374.5	83106.6	44922.3	58187.4	483763.1
13.31	38714.15	40901.39	30406.64	33298.46	48043.76
14.72	40562.24	50722.29	34698.97	21096.03	27559.64
15.68	28760.52	20871.79	32816.79	37895.71	45856.27

Overall, under the influence of long-period waves, the minimum tilt-resistant safety coefficients of offshore wind farms are higher than the standardized tilt-resistant safety coefficients in different wind and wave directions, and they have good overturning resistance.

5.2 Slip Resistance

The anti-slip stability of offshore structures is measured according to the slip resistance and slip force of the platform, and the slip safety coefficient regulated for offshore oil wells should be not less than 1.6. The five directions of action selected for the combination of waves and currents are the same as those above, and the slip force of offshore wind farms under the influence of waves with five different directions of action is shown in Table 3. When the period of the waves is 12.52s and 14.72s, the slip force is maximum at 180° in the wave direction, which is 389.6 and 315.3, respectively. When the wave period is 12.52s and 14.72s, the slip force is maximum at 180°, which is 389.6 and 315.3, respectively, and when the wave period is 13.31s and 15.68s, the slip force is maximum at 90° and 64.2°, which is 281.9 and 259.9, respectively.

Table 3. Skid force

Wave cycle(s)	Skid force				
	0°	90°	64.2°	180°	244.2°
12.52	237.3	368.5	208.1	389.6	187.4
13.31	277.6	281.9	226.5	232.1	270.2
14.72	286.7	223.8	129.8	315.3	155
15.68	142.1	232.6	259.9	119.2	222.4

The anti-slip resistance of offshore wind farms is shown in Table 4. The minimum anti-slip resistance of different long-period waves in five wave directions corresponds to the maximum slip force when the wave period is 12.52s, 14.72s, the minimum anti-slip resistance in the wave direction of 180 °, respectively, 2036.28, 761.2. Slip force is at its maximum; the anti-slip resistance is at its minimum; offshore wind farms are in the most dangerous situation; the anti-slip calibration, respectively, can get the anti-slip safety coefficient, 5.23, 2.41, are greater than 1.6, are greater than 1.6. In addition,

when the wave period is 13.31s and 15.68s, the slip resistance is the smallest at 90° and 64.2° in the wave direction, which is 895.04 and 643.43, and the corresponding slip resistance is 3.18 and 2.18, which is the smallest at 180° in the wave direction. The safety coefficients are 3.18 and 2.48, which are higher than the standardized safety coefficients.

Table 4. Anti-skid force

Wave cycle(s)	Anti-skid force				
	0°	90°	64.2°	180°	244.2°
12.52	2640.71	1936.94	2409.95	2036.28	2204.98
13.31	799.48	895.04	1889.01	1838.472	1613.09
14.72	1126.73	1855.3	1768.41	761.2	1071.05
15.68	1050.11	976.86	643.43	1399.32	858.46

Under the influence of long-period waves, the minimum slip-resistant safety coefficient of offshore wind farms is higher than the standardized tilt-resistant safety coefficient in different wind and wave directions and has a good performance in slip-resistant and stable mobility.

6 Conclusion

This paper establishes a numerical model of long-period wave impact on offshore wind power structures, then compares the numerical simulation and experimental results with the actual analysis of the impact toughness of offshore wind farms, and draws the following conclusions: (1) A numerical wave flume model is established, and the numerical results are compared with the actual simulation tests.

1) A numerical wave flume model is established to simulate the impact of long-period waves on offshore wind power structures, and the numerical results are compared and verified with the actual simulation experiments. The numerical simulation results can reproduce the wave impact process of the physical experiments, and the numerical results of the alternating process of the impact pressure are also consistent with the experimental values so that the long-period waves encountered by offshore wind power structures are simulated well. Structure encountered by the long-period wave impact.

2) Evaluation of impact toughness of offshore structure example - 202MW offshore wind farm in Jiangsu, China, offshore Langshui, in terms of tilt stability, an offshore wind farm in the long-period wave impact, the tilt safety factor in different directions of the wave is greater than 1.4, higher than the normative tilt safety factor, and in terms of slip stability, an offshore wind farm in the long-period wave impact, the tilt safety factor is greater than 1.4, higher than the normative tilt safety factor. Overall, offshore wind farms have good impact toughness in the face of long-period wave impacts.

Funding:

This research was supported by the Analysis of Wave power resources in key coastal areas of Guangdong Province based on refined simulation data, 202002030248

References

[1] Wang, X. L., Wang, Z. Q., Ma, X. P., Subramanian, S. V., & Li, X. C. (2018). Analysis of impact toughness scatter in simulated coarse-grained haz of e550 grade offshore engineering steel from the aspect of crystallographic structure. Materials Characterization, 140.

[2] Wen, B., Dong, X., Tian, X., Peng, Z., & Wei, K. (2018). The power performance of an offshore floating wind turbine in platform pitching motion. Energy, 154.

[3] Gao, Y., Zhu, J., Wang, L., & Li, W. (2023). Experimental investigation of breaking regular waves slamming on offshore wind jacket structure. Ocean engineering.

[4] Liu, D., Yang, J., & Zhang, Y. (2022). Toughness and fracture mechanism at low temperature of offshore engineering steel at different welding heat inputs. Metallurgical Research & Technology, 119(4), 405.

[5] Richmond, M., Smolka, U., & Kolios, A. (2020). Feasibility for damage identification in offshore wind jacket structures through monitoring of global structural dynamics. Energies, 13.

[6] Dan, L., & Weixing, Y. (2011). Two-level optimization for gfrp wind turbine blade structural design. Journal of Nanjing University of Aeronautics & Astronautics, 43(5), 598-601.

[7] Chih-Hua, Keni, Wu, Vinh-Tan, & Nguyen. (2017). Aerodynamic simulations of offshore floating wind turbine in platform-induced pitching motion. Wind Energy.

[8] Canming, C., Xiaodong, S. U., Jianxin, H. E., Xipeng, W., & Weilan, H. (2018). Study on horizontal bearing capacity of large diameter wing-monopile of offshore wind turbine. The Ocean Engineering.

[9] Ilson, D. S. J. F., Viana Cardoso, O. C., Cunha, G. T., & Luiz, P. D. A. A. (2022). Coupling soil-fluid-structure domains by localized lagrange multipliers mixed formulation (u, p) for modeling offshore wind turbine vibration. International journal of computational methods.

[10] Page, A. M., Naess, V., De Vaal, J. B., Eiksund, G. R., & Nygaard, T. A. (2019). Impact of foundation modelling in offshore wind turbines: comparison between simulations and field data. Marine Structures, 64(MAR.), 379-400.

[11] Xie, S., Jin, X., He, J., & Zhang, C. (2019). Structural responses suppression for a barge-type floating wind turbine with a platform-based tmd. IET Renewable Power Generation, 13(13), 2473-2479.

[12] Liu, X., Jiang, D., Liufu, K., Fu, J., Liu, Q., & Li, Q. (2022). Numerical investigation into impact responses of an offshore wind turbine jacket foundation subjected to ship collision. Ocean Engineering, 248, 110825-.

[13] Shittu, A. A., Mehmanparast, A., Shafiee, M., Kolios, A., & Pilario, K. (2020). Structural reliability assessment of offshore wind turbine support structures subjected to pitting corrosion-fatigue: a damage tolerance modelling approach. Wind Energy.

[14] Oh, K. Y., Nam, W., Ryu, M. S., Kim, J. Y., & Epureanu, B. I. (2018). A review of foundations of offshore wind energy convertors: current status and future perspectives. Pergamon.

[15] Shi, W., Liu, Y., Wang, W., Cui, L., & Li, X. (2023). Numerical study of an ice-offshore wind turbine structure interaction with the pile-soil interaction under stochastic wind loads. Ocean engineering.

[16] Hammer T, C., Willems, T., Hendrikse H. (2023). Dynamic ice loads for offshore wind support structure design. Marine structures.

[17] Ji, X., Tian, Z., Song, H., & Liu, F. (2022). Structural performance degradation identification of offshore wind turbines based on variational mode decomposition with a grey wolf optimizer algorithm. Ocean engineering.

[18] A, L. Z., A, P. H., A, S. C., A, M. L., B, H. Z., & A, H. Y., et al. Structural health monitoring of offshore wind power structures based on genetic algorithm optimization and uncertain analytic hierarchy process - sciencedirect. Ocean Engineering, 218.

[19] Sun, C., & Jahangiri, V. (2019). Fatigue damage mitigation of offshore wind turbines under real wind and wave conditions - sciencedirect. Engineering Structures, 178, 472-483.

[20] Stber, U., & Thomsen, F. (2021). How could operational underwater sound from future offshore wind turbines impact marine life?. The Journal of the Acoustical Society of America, 149(3), 1791-1795.

[21] Maria, Martinez-Luengo, Athanasios, Kolios, Lin, & Wang. (2017). Parametric fea modelling of offshore wind turbine support structures: towards scaling-up and capex reduction. International Journal of Marine Energy.